The Astrophysical Journal, 602:850–859, 2004 February 20

DISCOVERY OF A MASSIVE PROTOSTAR NEAR IRAS 18507+0121

D. S. Shepherd,[1] D. E. A. Nürnberger,[2] and L. Bronfman[3]

Received 2003 July 29; accepted 2003 October 24

ABSTRACT

We have observed the massive star-forming region IRAS 18507+0121 at millimeter wavelengths in 3 mm continuum emission, $H^{13}CO^+$ ($J = 1-0$) and SiO ($v = 0$, $J = 2-1$) line emission, and at near-infrared (NIR) wavelengths between 1.2 and 2.1 μm. Two compact molecular cores are detected: one north and one south, separated by $\sim 40''$. The northern molecular core contains a newly discovered, deeply embedded, B2 protostar surrounded by several hundred solar masses of warm gas and dust, G34.4+0.23 MM. Based on the presence of warm dust emission and the lack of detection at NIR wavelengths, we suggest that G34.4+0.23 MM may represent the relatively rare discovery of a massive protostar (e.g., analogous to a low-mass "Class 0" protostar). The southern molecular core is associated with an NIR cluster of young stars and an ultracompact H II region, G34.4+0.23, with a central B0.5 star. The fraction of NIR stars with excess infrared emission indicative of circumstellar material is greater than 50%, which suggests an upper limit on the age of the IRAS 18507+0121 star-forming region of 3 Myr.

Subject headings: H II regions — ISM: molecules — stars: formation — stars: pre–main-sequence

On-line material: machine-readable table

1. INTRODUCTION

The massive star-forming region associated with IRAS 18507+0121 (hereafter IRAS 18507) is located 3.9 kpc from the Sun and is roughly $11'$ from the H II region complex G34.3+0.2 (Molinari et al. 1996; Carral & Welch 1992). Near IRAS 18507, Miralles, Rodríguez, & Scalise (1994) discovered an ultracompact (UC) H II region (G34.4+0.23) embedded in a 1000 $M_\odot$ molecular cloud traced by NH_3 emission. The NH_3 emission is elongated in the north-south direction, with a total extent of about $7'$; however, the $1.'5$ resolution of the observations was not adequate to discern the structure of the core (Miralles et al. 1994). The detection of unresolved HCO^+ and SiO emission (half-power beamwidth [HPBW] of $55''$ and $43''$, respectively) is reported by Richards et al. (1987) and Harju et al. (1998).

IRAS 18507 was detected in a CS ($J = 2-1$) survey of *IRAS* point sources with far-infrared colors suggestive of UC H II regions (Bronfman, Nyman, & May 1996). The source was selected for further high-resolution studies because of its broad line wings, a signature of current star formation. By modeling HCO^+, $H^{13}CO^+$, CS, and $C^{34}S$ spectra obtained at an angular resolution of $\sim 16''$, Ramesh, Bronfman, & Deguchi (1997) demonstrate that the observed line profiles can be explained by a collapsing hot core of about 800 $M_\odot$, which is hidden behind a cold ($\sim$4 K) and dense (3×10^4 cm^{-3}) envelope of about 200 $M_\odot$. The IRAS 18507 region is also associated with variable H_2O maser (Scalise, Rodríguez, & Mendoza-Torres 1989; Palla et al. 1991; Miralles et al. 1994) and CH_3OH maser emission (Schutte et al. 1993; Szymczak, Hrynek, & Kus 2000). Molinari et al. (1996, 1998) observed IRAS 18507 (labeled "Mol 74" in their papers) and estimated a deconvolved size of the UC H II region of $0.''7$ (0.013 pc at $D = 3.9$ kpc).

To date, the molecular gas and near-infrared (NIR) emission have not been observed with arcsecond resolution. Given the distance to the source of nearly 4 kpc, the current low-resolution observations have not made it possible to determine the evolutionary status of the region or the relationship between the *IRAS* source, the UC H II region, and the molecular gas. In this work, we present observations of IRAS 18507 at NIR wavelengths, in millimeter continuum emission tracing warm dust, and in the dense core tracer $H^{13}CO^+$ ($J = 1-0$) and the shock tracer SiO ($v = 0$, $J = 2-1$) with $\sim 5''$ resolution.

2. OBSERVATIONS

2.1. *Observations in the* 3 mm *Band*

Simultaneous observations in the 3 mm continuum band and $H^{13}CO^+$ ($J = 1-0$) and SiO ($v = 0, J = 2-1$) lines were made with the Owens Valley Radio Observatory (OVRO) array of six 10.4 m telescopes on 1998 April 19 and 1998 May 17. Projected baselines ranging from 12 to 120 m provided sensitivity to structures up to about $20''$ with $\sim 5''$ resolution. The total integration time on source was approximately 6.4 hr. Cryogenically cooled SIS receivers operating at 4 K produced typical single-sideband system temperatures of about 400 K. The gain calibrator was the quasar 1749+096, and the passband calibrators were 3C 454.3 and 3C 273. Observations of Neptune provided the flux density calibration scale, with an estimated uncertainty of $\sim$15%. Calibration was carried out using the Caltech MMA data reduction package (Scoville et al. 1993). Images were produced using the MIRIAD software package (Sault, Teuben, & Wright 1995) and deconvolved with a CLEAN-based algorithm.

Continuum images with a 1 GHz bandwidth centered at frequency 89.983 GHz have a synthesized beam of $4.''9 \times 4.''2$ (FWHM) at P.A. $-31.^\circ 2$ and rms noise of 3.3 mJy beam^{-1}. The spectral bandpass for $H^{13}CO^+$ and SiO is centered on the systemic local standard of rest velocity (v_{LSR}), 57.0 km s^{-1}. The $H^{13}CO^+$ images have a synthesized beam of $5.''3 \times 4.''5$ (FWHM) at P.A. $-43.^\circ 8$, spectral resolution of 1.728 km s^{-1},

[1] National Radio Astronomy Observatory, P.O. Box O, 1003 Lopezville Road, Socorro, NM 87801.
[2] European Southern Observatory, Casilla 19001, Santiago 19, Chile.
[3] Departamento de Astronomía, Universidad de Chile, Casilla 36-D, Santiago, Chile.

and rms noise of 50.0 mJy beam^{-1}. The SiO images have a synthesized beam of $5\farcs3 \times 4\farcs5$ (FWHM) at P.A. $-44\fdg1$ and rms noise of 45 mJy beam^{-1} at a spectral resolution of 1.738 km s^{-1}. SiO was not detected, and the images are not shown in this paper.

2.2. *Archival Observations at* 6 cm

Archival data from the National Radio Astronomy Observatory's Very Large Array (VLA)[4] were obtained at 4.88 GHz (6.15 cm) in continuum emission with a bandpass of 100 MHz.[5] Observations centered on IRAS 18507 were made on 1994 October 4 with an on-source integration time of about 4 minutes. The absolute flux scale was derived from observations of 3C 48, while the quasars 1801+010 and 1821+107 were used as gain calibrators. The data were calibrated and imaged using the AIPS++ data reduction package. The image had a synthesized beam of $5\farcs65 \times 2\farcs98$ (FWHM) at P.A. $60\fdg1$ and rms noise of 0.19 mJy beam^{-1}. Our resulting image is comparable to the AIPS-generated image from Molinari et al. (1998).

2.3. *NIR Observations*

Broadband J, H, and K' ($\lambda_c = 1.25$, 1.65, and 2.10 μm, respectively) observations were performed in 1999 May at the Las Campanas 2.5 m Du Pont Telescope using the facility NIR camera (Persson et al. 1992) equipped with a NICMOS 3 256×256 HgCdTe array detector. The chosen plate scale of $0\farcs348$ pixel^{-1} provides a field of view of about $90'' \times 90''$, thus covering an area of 1.7×1.7 pc at the distance of IRAS 18507 (3.9 kpc).

To remove randomly distributed cosmic rays, we applied a dithering method using $20''$–$25''$ offsets. In each filter the exposure time was 10 s per frame, resulting in an on-source integration time of up to 70 s. During acquisition of the data set we had photometric conditions throughout the night, and the seeing was $0\farcs6$–$0\farcs8$ FWHM. For photometric calibration we observed the faint NIR standard stars 9175 (=S071-D) and 9137 (=S372-S) from the sample of Persson et al. (1998).

Following the procedure given by Persson et al. (1998), data reduction (e.g., dark current subtraction, flat-fielding, bad-pixel correction, and sky subtraction) was performed using standard IRAF software packages. The Digitized Sky Surveys (1 and 2) and the *HST* Guide Star Catalog (both provided by the Space Telescope Science Institute) were used to obtain astrometric calibration with an accuracy better than $\pm 1''$. The detection limits in the NIR images are $J = 19.6$ mag, $H = 19.2$ mag, and $K' = 18.6$ mag. Because of relatively high readout noise, the quality of the photometric calibration is restricted to $\sigma_J = 1.2 \pm 0.5$ mag, $\sigma_H = 1.4 \pm 0.6$ mag, and $\sigma_{K'} = 1.6 \pm 0.6$ mag.

3. RESULTS

A single unresolved, newly discovered millimeter continuum source, G34.4+0.23 MM (hereafter G34.4 MM), is detected at $\alpha = 18^{\rm h}53^{\rm m}18\fs01$, $\delta = +01\arcdeg25'25\farcs6$ (J2000.0), with a total flux density of 56.8 mJy (Fig. 1). The 6 cm continuum image showing free-free emission from ionized gas is also shown in Figure 1 (Molinari et al. 1998). Coincident with G34.4 MM is a marginal detection of a 6 cm source with a flux density of 0.7 mJy (3.5 σ). The unresolved UC H II region, G34.4031+0.2276, discovered by Molinari et al. (1998) is located about $40''$ south of the millimeter core, at $\alpha = 18^{\rm h}53^{\rm m}18\fs68$, $\delta = +01\arcdeg24'47\farcs2$ (J2000.0), and has a flux density of 9.0 mJy.

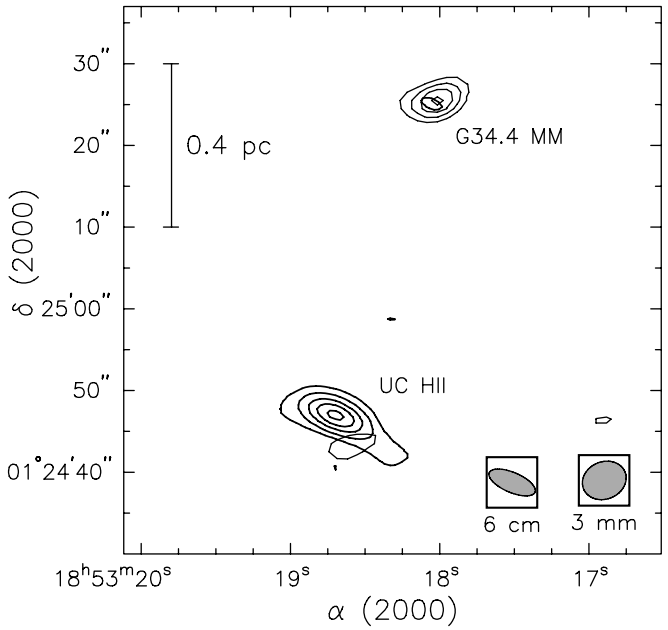

FIG. 1.—Millimeter (*thin contours*) and centimeter (*thick contours*) continuum emission toward IRAS 18507. The 3 mm image has an rms of 3.3 mJy beam^{-1} and a peak flux density of 32.0 mJy beam^{-1} at the position of G34.4 MM. Thin contours are plotted at ± 3, 5, 7, and 9 σ. The 6 cm image has an rms of 0.19 mJy beam^{-1} and a peak flux density of 8.72 mJy beam^{-1}. Thick contours are plotted at ± 3, 10, 20, 30, and 40 σ. Synthesized beams for both observations are plotted in the bottom right corner. A scale size of 0.4 pc is represented by a bar in the upper left corner.

The total $H^{13}CO^+$ flux density from 53.54 to 62.16 km s^{-1} is 33.64 Jy (Fig. 2). The strongest $H^{13}CO^+$ peak is located $\sim 3''$ northwest of the G34.4 UC H II region. A second $H^{13}CO^+$ peak is coincident with G34.4 MM. The two peaks are connected by a band of more diffuse molecular gas traced by $H^{13}CO^+$. The total extent of the dense $H^{13}CO^+$ gas is consistent with previous NH_3 observations made at $1\farcm5$ resolution (Miralles et al. 1994).

SiO ($J = 2 - 1$) emission is not detected, with a 3 σ upper limit of 135 mJy beam^{-1}. This is in contrast to the single-dish SiO spectrum ($43''$ resolution) obtained by Harju et al. (1998), in which they detect a 5 σ peak intensity of 0.26 K ($\sim$840 mJy). However, this discrepancy could be explained if the SiO emission were spatially extended and thus missed by our interferometric observations. Indeed, observations of IRAS 18507 by one of us (L. B.) at $16''$ resolution with the Nobeyama 45 m telescope show extended SiO emission with an FWHM of about $1'$. At the position of IRAS 18507 the spectrum is non-Gaussian, with a peak temperature of $\sim$0.7 K (1.1 Jy beam^{-1}) and a total measured velocity extent at zero intensity of $\sim$15 km s^{-1}. Assuming that the peak emission scales with the area of the synthesized beam, we would expect to detect a peak flux density of roughly 110 mJy beam^{-1} (2.4 σ) with our $5''$ resolution. However, our interferometric observations are only sensitive to structures up to $\sim 20''$, and

[4] The NRAO is a facility of the National Science Foundation operated under cooperative agreement by Associated Universities, Inc.

[5] Originally published by Molinari et al. (1998); however, their image did not include the position of the millimeter core. Thus, we have recalibrated and imaged their data to obtain a limit on the free-free continuum emission toward the millimeter core.

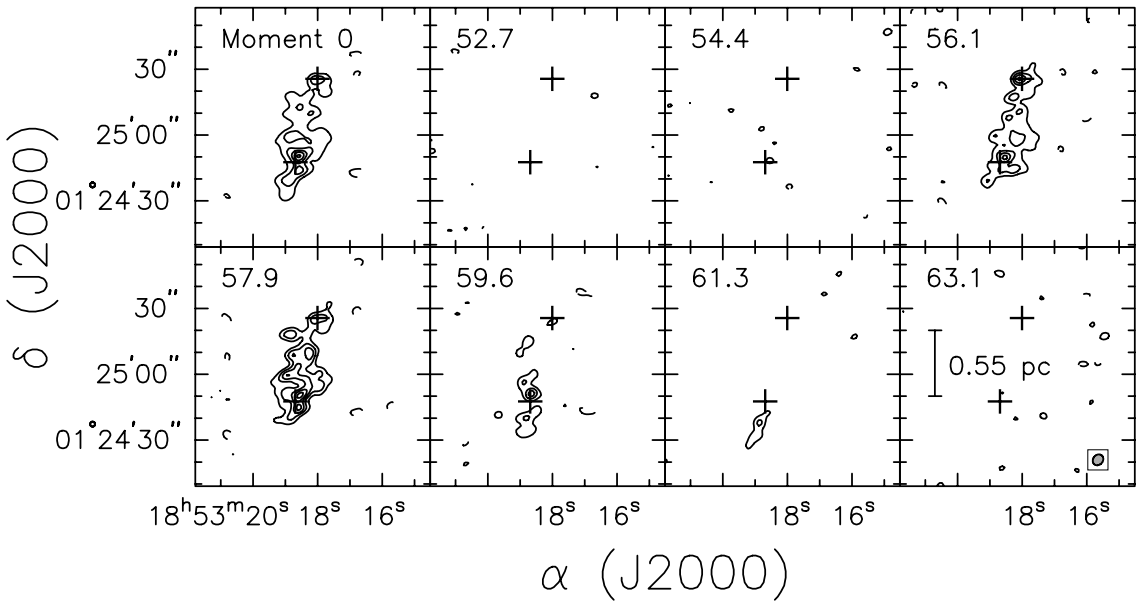

FIG. 2.—$H^{13}CO^+$ emission. The top left panel shows integrated $H^{13}CO^+$ emission (moment 0) between 55.25 and 62.15 km s^{-1} ($v_{LSR} = 57$ km s^{-1}). The rms in the image is 230 mJy beam^{-1} km s^{-1}; contours are plotted at ± 3, 5, 7, 9, and 11 σ. The remaining panels show the $H^{13}CO^+$ channel maps at 1.7 km s^{-1} spectral resolution. The central velocity is indicated in the top left corner of each panel. The channel rms is 50 mJy beam^{-1}, and contours are plotted at ± 3, 5, 7, 9, and 11 σ. The bottom right panel shows the synthesized beam in the bottom right corner ($5\farcs34 \times 4\farcs51$ at P.A. $-43\fdg8$) and a scale size of 0.55 pc. Plus signs represent the locations of the 6 cm continuum peak and G34.4 MM.

the actual source size is nearly 1′ FWHM. Thus, our lack of detection in SiO ($J = 2-1$) is likely due to a combination of the interferometer missing zero-spacing flux and low sensitivity to any remaining compact emission.

NIR images of the region are shown in Figure 3, while a comparison between the 2.10 μm emission and the $H^{13}CO^+$ emission is shown in Figure 4. An NIR cluster of young stars is located on the western edge of the southern $H^{13}CO^+$ core. The brightest member of the cluster (labeled "#54" in Figs. 3 and 4) has NIR magnitudes of $J = 17.0 \pm 0.6$ mag, $H = 15.3 \pm 0.5$ mag, and $K' = 14.2 \pm 0.4$ mag. The G34.4 UC H II region appears to be a member of this young stellar cluster, although it is not detected at 2.10 μm. In contrast, the northern $H^{13}CO^+$ core does not have an associated stellar cluster, nor is the exciting star of G34.4 MM detected in the NIR.

In Table 1, we summarize the results of the *JHK′* imaging. For all detected sources we list in columns (2) and (3) the positional offsets (in arcseconds) relative to the position of the brightest member of the cluster (source 54), as well as, in columns (4) and (5) the absolute coordinates. Finally, columns (6)–(8) contain the *J*-, *H*-, and *K′*-band magnitudes. As already mentioned above, typical photometric errors are in the range $\sigma_J = 1.2 \pm 0.5$ mag, $\sigma_H = 1.4 \pm 0.6$ mag, and $\sigma_{K'} = 1.6 \pm 0.6$ mag. In total we have detected 146 sources; however, 80 of them are only seen in the *K′* data, which suggests that the extinction is so large that many cluster members are too heavily extincted to be detectable at wavelengths shorter than 2 μm. Forty-three sources are detected in all three filters, which enabled us to calculate corresponding $J-H$, $H-K'$ and $J-K'$ colors. Assuming a distance of 3.9 kpc but not taking into account any possible foreground extinction, we also derive lower limits for the absolute magnitudes M_J, M_H, and $M_{K'}$.

The NIR colors and absolute magnitudes allow us to place the sources in NIR two-color and color-magnitude diagrams (see Figs. 5 and 6). In both diagrams the location of source 54 is indicated by an asterisk[6] and, using the extinction transformations given by Rieke & Lebofsky (1985), a reddening vector for $A_V = 5$ mag is given. In the $(H-K')$–$(J-H)$ diagram, the loci of the observed sources are compared to those of dwarfs and giants (*thick and thin lines, respectively*; Koornneef 1983). Similarly, in the M_J–$(J-K')$ diagram we mark the loci of stars on the main sequence (*thick line*) and the pre–main sequence at ages 0.3 and 3 Myr (*dashed lines*; Palla & Stahler 1993).

As noted by Strom, Strom, & Merrill (1993), low-mass stars possessing NIR excess emission usually populate three distinct regions of the $(H-K')$–$(J-H)$ diagram: sources associated with low excess emission (so-called weak-line T Tauri stars) are found in zone I, while zones II and III feature sources with high excess emission caused by circumstellar disks (classical T Tauri stars) and surrounding envelopes (protostars), respectively. The same, or at least a similar, scenario probably holds for intermediate- and high-mass stars (Nürnberger 2003). For about 50% of our sources with *JHK′* detections, we find that the NIR colors clearly offset from those of main-sequence stars; e.g., source 54 is extincted by almost $A_V = 20$ mag. Their reddening might be convincingly explained by intrinsic extinction due to the presence of relatively large amounts of circumstellar gas and dust. The other 50% of our *JHK′*-detected sources have colors that are reddened by at most 2–3 mag (likely as a result of foreground extinction) and, apart from that, appear to be consistent with those of main-sequence stars.

4. DISCUSSION

4.1. *Ionized Gas Emission*

The UC H II region G34.4+0.23 is detected at 6 cm with a flux density of 9 ± 0.2 mJy, while G34.4 MM has an unresolved 0.7 ± 0.2 mJy 6 cm continuum peak associated

[6] Note that source 54 is shown in the figures only to give a reference point to the brightest NIR member of the cluster and to allow the reader to relate positional offsets from source 54 given in Table 1 to other sources in the field.

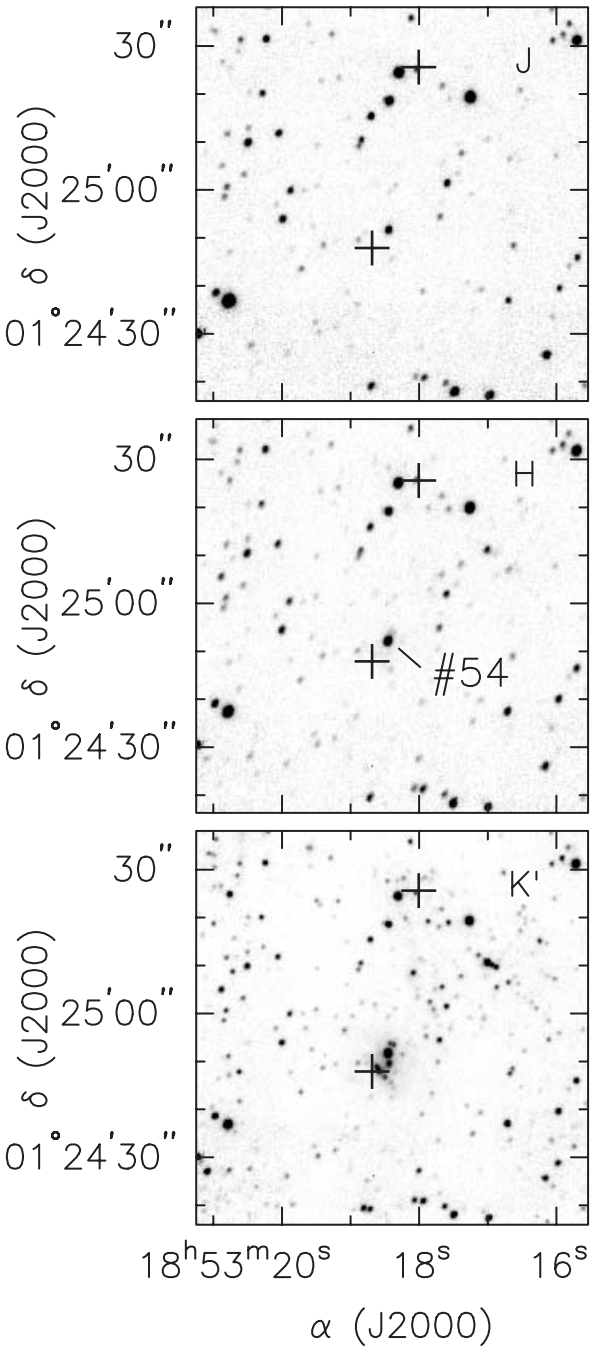

FIG. 3.—NIR images of the IRAS 18507 star-forming region in the broad bands J (*top*; 1.25 μm), H (*middle*; 1.65 μm), and K' (*bottom*; 2.10 μm). Plus signs represent the locations of the 6 cm continuum peak and G34.4 MM. The location of the NIR source 54 is shown in the middle panel.

with it. Thus, there are one or more early-type stars producing ionized gas toward both sources. Following the method outlined by Wood & Churchwell (1989), the physical properties of the ionized gas are calculated and presented in Table 2. For each source, the values listed are S_ν, the measured flux density at 4.8851 GHz; Δs, the line-of-sight depth at the peak position (an upper limit for unresolved sources); T_b, the synthesized beam brightness temperature; τ_ν, the optical depth, assuming that the beam is uniformly filled with $T_e = 10^4$ K ionized gas; EM, the emission measure; n_e, the rms electron density; U, the excitation parameter of the ionized gas; $N_{\rm L}$, the number of Lyman continuum photons required to produce the observed emission, assuming an ionization-bounded, spherically symmetric, homogeneous H II region; and finally, the spectral type of the central star, assuming that a single zero-age main-sequence (ZAMS) star is producing the observed Lyman continuum flux (Panagia 1973). These estimates should be considered a lower limit if there is significant dust absorption within the H II region or if the emission is being quenched by high accretion rates expected for OB protostars (e.g., Churchwell 1999 and references therein).

The values listed in Table 2 do not take into account possible dust absorption within the ionized gas, which would tend to underestimate $N_{\rm L}$, and hence the spectral type of the star. Estimates for G34.4 MM could also be uncertain by up to 50% because of the low–signal-to-noise ratio detection at 6 cm (3.5 σ). Despite these uncertainties, the derivations are probably accurate to within a spectral type. Comparison of the values in Table 2 with those in Wood & Churchwell (1989, their Table 17), shows that the physical parameters of the ionized gas in the G34.4 sources are consistent with those of ZAMS stars with spectral types later than B0. Values for the UC H II region G34.4+0.23 are consistent with those derived by Molinari et al. (1998) to within the errors.

4.2. *Thermal Dust Emission at Millimeter Wavelengths*

The UC H II region G34.4+0.23 has no detectable millimeter continuum emission coincident with the ionized gas peak. Further, members of the NIR cluster also show no millimeter continuum emission coincident with the stellar positions. The 3 σ upper limit on warm dust emission is $\sim$10 mJy beam^{-1}. The mass of gas and dust is estimated from the millimeter continuum emission using $M_{g+d} = F_\nu D^2/[B_\nu(T_d)\kappa_\nu]$, where D is the distance to the source, F_ν is the continuum flux density due to thermal dust emission at frequency ν, and B_ν is the Planck function at temperature T_d (Hildebrand 1983). The

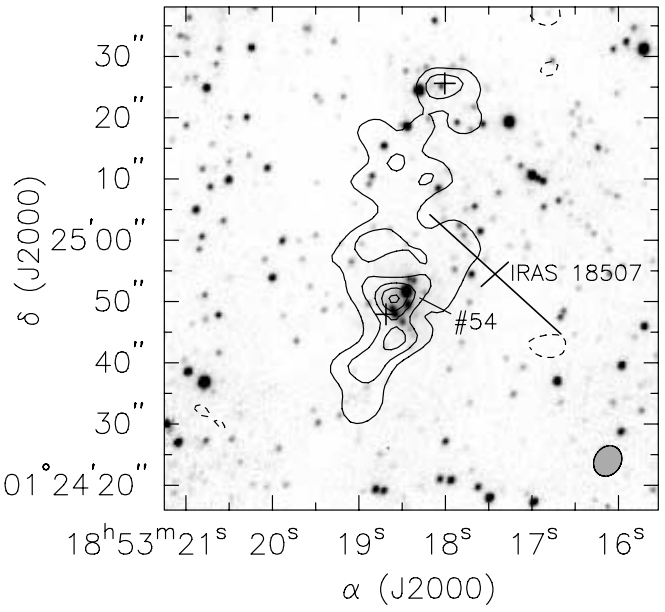

FIG. 4.—K' image (Fig 3) in gray scale compared with a map of the integrated $H^{13}CO^+$ emission between 55.25 and 62.15 km s^{-1} (Fig. 2, *top left panel*). Plus signs represent the locations of the 6 cm continuum peak and G34.4 MM; source 54 also identified. The location of IRAS 18507+0121 is illustrated by the cross centered at $\alpha = 18^{\rm h}53^{\rm m}17^{\rm s}.42$, $\delta = +01^\circ24'54''.5$ (J2000.0). The length and orientation of the symbol represents the positional accuracy.

TABLE 1

POSITIONS AND JHK' PHOTOMETRY OF ALL DETECTED SOURCES

Source (1)	Δx (arcsec) (2)	Δy (arcsec) (3)	R.A. (J2000.0) (4)	Decl. (J2000.0) (5)	J (mag) (6)	H (mag) (7)	K' (mag) (8)
1.....	−14.4	−33.7	18 53 17.48	+01 24 18.1	16.5	15.8	15.6
2.....	40.2	−32.9	18 53 21.12	+01 24 18.9	...	...	18.1
3.....	7.5	−32.7	18 53 18.94	+01 24 19.1	...	...	18.1
4.....	3.9	−32.5	18 53 18.70	+01 24 19.3	...	...	15.9
5.....	5.3	−32.3	18 53 18.79	+01 24 19.5	...	...	15.8
6.....	−12.4	−31.9	18 53 17.61	+01 24 19.9	18.2	17.3	16.6
7.....	24.2	−31.9	18 53 20.06	+01 24 19.9	...	...	18.2
8.....	−2.5	−31.7	18 53 18.27	+01 24 20.0	...	...	18.3
9.....	38.0	−31.7	18 53 20.98	+01 24 20.1	18.8	18.0	...
10.....	20.9	−31.6	18 53 19.84	+01 24 20.2	...	...	18.0
11.....	40.0	−31.1	18 53 21.11	+01 24 20.7	...	...	18.4
12.....	35.9	−29.6	18 53 20.84	+01 24 22.2	18.4	17.5	...
13.....	−11.3	−29.2	18 53 17.69	+01 24 22.5	...	...	18.4
14.....	28.8	−27.9	18 53 20.36	+01 24 23.9	...	...	18.2
15.....	−36.1	−27.8	18 53 16.04	+01 24 24.0	...	...	17.7
16.....	4.6	−26.6	18 53 18.75	+01 24 25.2	...	...	18.3
17.....	32.4	−26.1	18 53 20.61	+01 24 25.7	18.5	17.9	...
18.....	−34.4	−26.1	18 53 16.15	+01 24 25.7	16.8	16.5	16.2
19.....	22.1	−25.7	18 53 19.91	+01 24 26.1	19.4	18.6	17.6
20.....	39.5	−24.7	18 53 21.07	+01 24 27.1	...	18.3	15.8
21.....	−6.7	−24.5	18 53 18.00	+01 24 27.3	...	18.2	17.0
22.....	30.2	−24.2	18 53 20.45	+01 24 27.6	18.9	18.3	17.9
23.....	30.0	−23.7	18 53 20.44	+01 24 28.1	19.5	...	...
24.....	−37.1	−22.9	18 53 15.96	+01 24 28.9	...	...	16.4
25.....	15.3	−21.5	18 53 19.46	+01 24 30.3	19.5	18.2	17.5
26.....	11.6	−20.3	18 53 19.21	+01 24 31.5	...	18.9	18.0
27.....	−40.6	−19.5	18 53 15.73	+01 24 32.3	...	...	17.8
28.....	−10.9	−18.3	18 53 17.71	+01 24 33.5	...	...	18.5
29.....	−18.5	−16.8	18 53 17.21	+01 24 34.9	...	18.6	17.7
30.....	6.8	−15.6	18 53 18.90	+01 24 36.2	...	...	18.4
31.....	35.0	−14.8	18 53 20.77	+01 24 37.0	14.5	14.3	14.1
32.....	−26.0	−14.7	18 53 16.71	+01 24 37.1	17.9	16.4	15.7
33.....	37.8	−13.1	18 53 20.96	+01 24 38.7	17.1	16.2	15.7
34.....	−7.4	−12.8	18 53 17.95	+01 24 39.0	...	...	18.3
35.....	−37.2	−12.1	18 53 15.96	+01 24 39.7	18.0	16.7	15.9
36.....	38.5	−11.3	18 53 21.00	+01 24 40.5	...	...	16.8
37.....	32.5	−10.1	18 53 20.61	+01 24 41.7	...	...	17.8
38.....	−9.5	−8.4	18 53 17.80	+01 24 43.4	...	...	18.2
39.....	19.0	−8.2	18 53 19.71	+01 24 43.6	18.9	18.2	17.9
40.....	−1.0	−7.2	18 53 18.37	+01 24 44.6	...	...	17.0
41.....	−0.6	−6.1	18 53 18.41	+01 24 45.7	...	18.3	16.5
42.....	−41.1	−5.7	18 53 15.70	+01 24 46.0	17.9	16.8	16.2
43.....	0.7	−4.9	18 53 18.48	+01 24 46.8	...	...	15.8
44.....	34.8	−4.6	18 53 20.76	+01 24 47.2	...	18.7	17.9
45.....	−26.6	−4.2	18 53 16.66	+01 24 47.6	...	...	16.7
46.....	32.5	−3.9	18 53 20.61	+01 24 47.9	...	...	16.9
47.....	2.0	−3.5	18 53 18.58	+01 24 48.2	...	...	15.4
48.....	14.2	−3.1	18 53 19.40	+01 24 48.7	19.0	18.3	18.3
49.....	−0.2	−2.1	18 53 18.43	+01 24 49.7	...	...	15.2
50.....	6.6	−2.1	18 53 18.88	+01 24 49.7	19.2	18.2	17.5
51.....	−10.9	−1.9	18 53 17.71	+01 24 49.9	...	...	18.1
52.....	34.9	−0.7	18 53 20.77	+01 24 51.0	...	...	17.5
53.....	−3.1	−0.3	18 53 18.24	+01 24 51.5	...	...	17.1
54.....	0.0	0.0	18 53 18.44	+01 24 51.8	17.0	15.3	14.2
55.....	−4.3	1.9	18 53 18.15	+01 24 53.7	...	...	18.0
56.....	23.2	2.2	18 53 19.99	+01 24 54.0	17.3	16.7	16.3
57.....	−11.2	2.7	18 53 17.69	+01 24 54.5	18.6	17.5	16.7
58.....	−35.1	2.8	18 53 16.11	+01 24 54.6	...	...	17.6
59.....	−8.3	3.5	18 53 17.89	+01 24 55.3	...	...	17.8
60.....	9.5	4.8	18 53 19.08	+01 24 56.5	...	...	17.6
61.....	−13.5	5.1	18 53 17.54	+01 24 56.9	...	...	18.4
62.....	24.5	5.1	18 53 20.08	+01 24 56.9	...	18.7	18.0
63.....	18.0	5.2	18 53 19.64	+01 24 56.9	...	...	18.5

TABLE 1—*Continued*

Source (1)	Δx (arcsec) (2)	Δy (arcsec) (3)	R.A. (J2000.0) (4)	Decl. (J2000.0) (5)	J (mag) (6)	H (mag) (7)	K' (mag) (8)
64.....	−35.0	6.7	18 53 16.11	+01 24 58.5	...	...	18.5
65.....	−20.9	7.2	18 53 17.05	+01 24 59.0	...	...	18.0
66.....	7.7	7.7	18 53 18.96	+01 24 59.5	...	...	18.6
67.....	21.5	8.1	18 53 19.88	+01 24 59.9	17.7	17.2	16.9
68.....	35.4	8.8	18 53 20.80	+01 25 00.6	18.2	17.4	17.1
69.....	−9.9	9.1	18 53 17.78	+01 25 00.9	...	...	17.1
70.....	−32.4	9.3	18 53 16.28	+01 25 01.1	...	...	18.0
71.....	−12.8	9.7	18 53 17.59	+01 25 01.5	17.5	17.1	16.8
72.....	2.9	10.1	18 53 18.64	+01 25 01.9	...	...	18.4
73.....	−31.4	10.5	18 53 16.35	+01 25 02.3	...	...	17.9
74.....	−9.2	10.6	18 53 17.83	+01 25 02.4	...	...	17.1
75.....	−4.8	11.1	18 53 18.12	+01 25 02.9	18.1	17.5	...
76.....	31.7	11.4	18 53 20.56	+01 25 03.2	19.0	18.1	17.5
77.....	−6.4	11.6	18 53 18.01	+01 25 03.4	...	...	18.2
78.....	−14.9	11.7	18 53 17.45	+01 25 03.5	...	...	18.5
79.....	−6.5	12.8	18 53 18.01	+01 25 04.6	18.4	...	...
80.....	36.4	13.2	18 53 20.87	+01 25 05.0	19.2	17.3	16.3
81.....	−10.4	13.3	18 53 17.76	+01 25 05.1	...	...	17.2
82.....	−23.7	13.7	18 53 16.86	+01 25 05.5	...	...	17.4
83.....	−11.8	13.8	18 53 17.66	+01 25 05.6	...	18.2	17.0
84.....	−28.4	14.4	18 53 16.55	+01 25 06.2	...	...	18.0
85.....	−26.3	14.7	18 53 16.69	+01 25 06.5	19.3	17.9	17.3
86.....	−36.4	15.4	18 53 16.02	+01 25 07.2	...	18.8	17.8
87.....	−27.6	15.8	18 53 16.60	+01 25 07.6	...	...	17.6
88.....	−34.8	16.0	18 53 16.12	+01 25 07.8	...	...	17.8
89.....	−5.5	16.7	18 53 18.08	+01 25 08.5	...	...	16.6
90.....	33.9	17.0	18 53 20.71	+01 25 08.7	...	...	17.1
91.....	−23.5	18.0	18 53 16.88	+01 25 09.8	...	...	15.7
92.....	30.8	18.1	18 53 20.50	+01 25 09.9	17.0	16.6	16.2
93.....	6.0	18.7	18 53 18.84	+01 25 10.5	17.7	17.1	16.8
94.....	−21.7	18.9	18 53 16.99	+01 25 10.7	...	16.9	15.1
95.....	−13.2	19.5	18 53 17.56	+01 25 11.3	19.6	18.0	...
96.....	−7.1	19.6	18 53 17.97	+01 25 11.4	...	...	18.2
97.....	24.1	20.0	18 53 20.05	+01 25 11.8	17.5	17.1	16.8
98.....	−19.7	20.4	18 53 17.12	+01 25 12.2	...	...	16.9
99.....	30.7	21.0	18 53 20.49	+01 25 12.8	19.1	18.4	17.9
100.....	27.3	22.1	18 53 20.26	+01 25 13.9	...	...	18.1
101.....	−34.6	22.9	18 53 16.14	+01 25 14.6	...	...	17.3
102.....	−33.1	23.4	18 53 16.24	+01 25 15.1	...	...	17.0
103.....	3.9	23.7	18 53 18.70	+01 25 15.5	17.3	16.9	16.6
104.....	−22.9	23.9	18 53 16.92	+01 25 15.7	...	...	18.5
105.....	−28.9	25.5	18 53 16.51	+01 25 17.3	...	...	18.0
106.....	−11.1	26.3	18 53 17.70	+01 25 18.1	...	...	17.7
107.....	−0.1	26.9	18 53 18.44	+01 25 18.7	16.3	16.0	15.6
108.....	38.1	27.0	18 53 20.98	+01 25 18.8	...	...	17.6
109.....	−29.9	27.1	18 53 16.44	+01 25 18.9	...	...	17.9
110.....	−8.7	27.4	18 53 17.87	+01 25 19.2	...	18.8	17.3
111.....	−30.0	27.8	18 53 16.44	+01 25 19.6	...	...	17.8
112.....	−17.7	28.0	18 53 17.26	+01 25 19.8	15.1	14.6	< 14
113.....	−3.8	28.1	18 53 18.20	+01 25 19.9	...	...	17.6
114.....	27.7	28.3	18 53 20.29	+01 25 20.1	18.0	17.4	17.1
115.....	30.6	28.3	18 53 20.48	+01 25 20.1	...	...	18.0
116.....	−11.6	30.0	18 53 17.67	+01 25 21.8	18.8	18.2	18.0
117.....	−29.6	30.4	18 53 16.47	+01 25 22.2	...	...	17.9
118.....	14.9	31.1	18 53 19.44	+01 25 22.9	...	19.0	17.5
119.....	11.0	31.6	18 53 19.18	+01 25 23.4	19.5	18.4	17.9
120.....	15.6	31.7	18 53 19.48	+01 25 23.5	...	...	17.5
121.....	−36.3	32.2	18 53 16.03	+01 25 24.0	...	...	18.2
122.....	−2.2	32.8	18 53 18.30	+01 25 24.5	15.4	15.0	14.7
123.....	34.6	33.1	18 53 20.75	+01 25 24.9	...	17.9	16.0
124.....	−6.0	33.4	18 53 18.04	+01 25 25.2	18.2	17.6	17.2
125.....	−27.2	33.5	18 53 16.63	+01 25 25.3	18.6	17.9	...
126.....	38.0	34.6	18 53 20.98	+01 25 26.4	...	...	17.6
127.....	36.5	34.8	18 53 20.88	+01 25 26.6	19.6	18.7	17.5

TABLE 1—*Continued*

Source (1)	Δx (arcsec) (2)	Δy (arcsec) (3)	R.A. (J2000.0) (4)	Decl. (J2000.0) (5)	J (mag) (6)	H (mag) (7)	K' (mag) (8)
128.....	−28.7	35.0	18 53 16.53	+01 25 26.8	19.2	18.5	...
129.....	0.1	35.8	18 53 18.45	+01 25 27.6	...	...	17.7
130.....	−2.1	36.0	18 53 18.31	+01 25 27.8	...	...	17.4
131.....	−9.3	36.1	18 53 17.82	+01 25 27.9	...	...	17.6
132.....	−3.4	36.4	18 53 18.22	+01 25 28.2	...	...	17.3
133.....	−8.0	36.5	18 53 17.91	+01 25 28.3	...	...	17.5
134.....	32.9	37.0	18 53 20.64	+01 25 28.8	19.5	18.3	17.6
135.....	−25.2	37.5	18 53 16.77	+01 25 29.3	...	18.8	17.6
136.....	−9.7	37.8	18 53 17.80	+01 25 29.6	...	...	18.0
137.....	37.9	38.7	18 53 20.97	+01 25 30.5	...	...	17.7
138.....	−35.8	39.3	18 53 16.06	+01 25 31.1	18.4	17.5	17.2
139.....	−41.0	39.4	18 53 15.71	+01 25 31.2	15.9	14.8	< 14
140.....	26.8	39.6	18 53 20.23	+01 25 31.4	17.4	16.7	16.3
141.....	−38.0	40.6	18 53 15.91	+01 25 32.4	18.4	17.1	16.5
142.....	12.5	40.7	18 53 19.28	+01 25 32.5	18.9	18.2	17.9
143.....	39.1	41.6	18 53 21.05	+01 25 33.3	...	...	17.1
144.....	17.2	42.8	18 53 19.58	+01 25 34.6	...	...	17.1
145.....	−39.3	42.9	18 53 15.82	+01 25 34.7	18.5	17.6	17.1
146.....	−39.4	45.7	18 53 15.82	+01 25 37.5	19.3	18.4	...

NOTES.—Units of right ascension are hours, minutes, and seconds, and units of declination are degrees, arcminutes, and arcseconds. Sources 41, 43, 47, 49, 50, 53, 54, and 55 are likely cluster members. Typical photometric errors are $\sigma_J \sim 1.2 \pm 0.5$ mag, $\sigma_H \sim 1.4 \pm 0.6$ mag, and $\sigma_{K'} \sim 1.6 \pm 0.6$ mag. Table 1 is also available in machine-readable form in the electronic edition of the *Astrophysical Journal*.

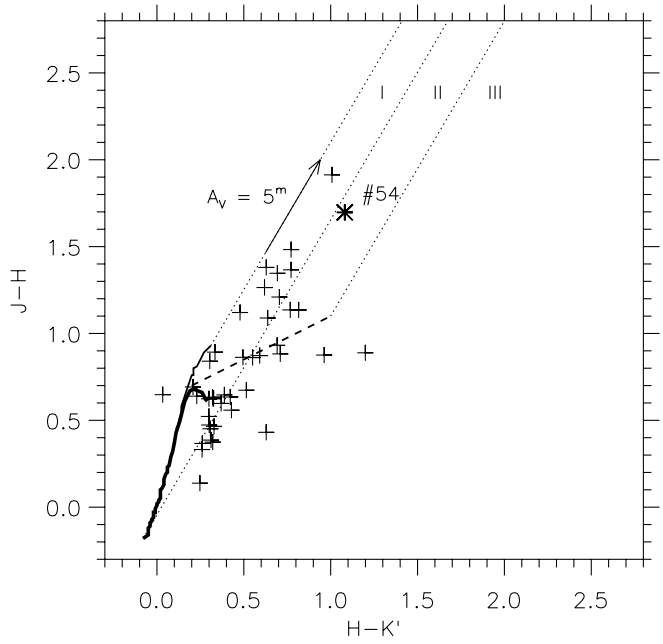

FIG. 5.—$(H-K')$–$(J-H)$ diagram of the detected NIR sources without applying any correction for possible foreground extinction. The location of source 54 is highlighted by an asterisk. Typical loci of dwarfs and giants are marked by the thick and thin lines, respectively. Further explanations are given in the text.

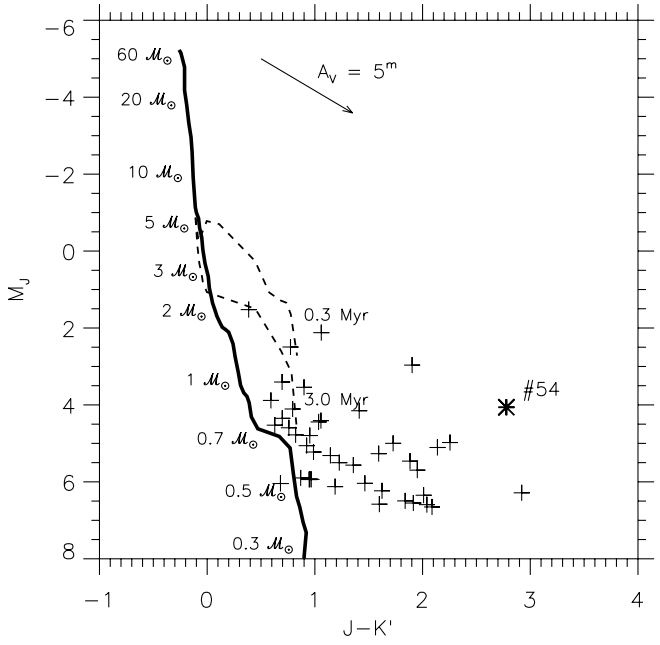

FIG. 6.—M_J–$(J-K')$ diagram of the detected NIR sources, again without applying any correction for possible foreground extinction. The location of source 54 is highlighted by an asterisk. Loci of stars on the main sequence (*thick line*) and on the pre–main sequence at ages of 0.3 and 3 Myr (*dashed lines*) are outlined.

TABLE 2
Derived Parameters for Ionized Gas Detected at 6 cm Wavelength

Source	S_ν[a] (mJy)	Δs (pc)	T_b (K)	τ_ν	EM (10^5 pc cm^{-6})	n_e (cm^{-3})	U (pc cm^{-2})	$\log N_{\rm L}$ (s^{-1})	Spectral Type
G34.4 MM	0.7	< 0.21	2.4	2.4×10^{-4}	2.1	$>10^3$	2.3	44.76	B2
G34.4+0.23	9.0	0.12[b]	31.0	3.1×10^{-3}	2.7	$>10^3$	5.3	45.87	B0.5

[a] Flux densities measured in the primary beam-corrected image.
[b] Deconvolved size from Molinari et al. 1998.

dust opacity per gram of gas is estimated from $\kappa_\nu = 0.006(\nu/245\ \mathrm{GHz})^\beta$ cm^2 g^{-1}, where β is the opacity index (see Kramer et al. 1998 and the discussion in Shepherd & Watson 2002). We assume that the emission is optically thin and that the temperature of the dust can be characterized by a single value. We take T_d to be 50 K, on the basis of measurements of typical conditions in warm molecular cores with embedded protostars (Hogerheijde et al. 1998), and $\beta = 1.5$ (Pollack et al. 1994). We also assume a distance of 3.9 kpc (Molinari et al. 1996) and a gas-to-dust ratio of 100 (Hildebrand 1983). Thus, the upper limit to the mass of gas and dust that can exist around the UC H II region and still be below our detection threshold is 40 $M_\odot$.

G34.4 MM has a strong millimeter continuum peak. Assuming that the ionized gas is optically thin between 6 cm and 3 mm ($S_\nu \propto \nu^{-0.1}$), we expect a contribution of 0.52 mJy to the flux density at 3 mm. Thus, the total flux density due to thermal dust emission at 3 mm is 56.3 mJy. We find that the mass of gas and dust associated with thermal dust emission at 3 mm is approximately 240 $M_\odot$. Changing the assumptions of T_d and β, we find that mass estimates vary from 150 $M_\odot$ with $T_d = 50$ K and $\beta = 1$ to as high as 650 $M_\odot$ with $T_d = 30$ K and $\beta = 2$. Despite the uncertainties associated with this estimate, our results show that there are several hundred solar masses of warm gas and dust in this region. Assuming that the G34.4 MM core is heated internally, this large molecular mass is consistent with the presence of a massive, embedded OB star or a cluster of massive stars (e.g., Saraceno et al. 1996).

4.3. $H^{13}CO^+$ *Emission*

To estimate the average column density and mass associated with the $H^{13}CO^+$ emission (Table 3), we assume that the $H^{13}CO^+$ is optically thin and that the rotational temperature follows the average kinetic temperature derived from NH_3 observations, e.g., $T_{\rm rot} = 22$ K (Molinari et al. 1996). Temperatures are likely to be higher in cores with embedded sources and lower in the diffuse gas; however, an average temperature of 22 K should be a reasonable estimate. Typical uncertainties are a factor of 2–3.

Abundances of $[HCO^+]/[H_2]$ in massive star-forming regions are typically $\sim 10^{-9}$ (Blake et al. 1987). Assuming an isotopic ratio $[HCO^+]/[H^{13}CO^+] \sim 51$ for the Galactocentric distance to IRAS 18507 of 5.8 kpc (Wilson & Rood 1994), we derive a total mass for the $H^{13}CO^+$ cloud of 5×10^4 $M_\odot$ and compact core masses of $(4\text{–}5) \times 10^3$ $M_\odot$. This estimate can easily be off by an order of magnitude if HCO^+, and hence $H^{13}CO^+$, is enhanced because of shocks. Comparing our mass estimates with that derived from NH_3 of 1000 $M_\odot$ and assuming that the $H^{13}CO^+$ and NH_3 trace the same volume of gas, our estimates are an order of magnitude larger, suggesting that some enhancement of the HCO^+ abundance has likely occurred in this region.

With $H^{13}CO^+$ column densities in hand, we can attempt to constrain the intrinsic extinction of the central sources of both molecular cores. Taking into account abundances and isotopic ratios as given above, the $H^{13}CO^+$ column densities of 2×10^{14} cm^{-2} convert into $N(H_2) \sim 10^{25}$ cm^{-2}. Following Bohlin, Savage, & Drake (1978), we relate the H_2 column densities and A_V via the formula $N(H_2)/A_V = 0.94 \times 10^{21}$ cm^{-2} mag^{-1}, for $A_V < 1$ mag. This suggests intrinsic extinctions of the order of 10^4 mag toward the central sources of the two G34.4 cores. We emphasize that these A_V values represent only rough estimates, because the given $N(H_2)/A_V$ relation might flatten significantly for $A_V \gg 1$ mag (see Dickman 1978 and Frerking, Langer, & Wilson 1982). Nevertheless, such large intrinsic extinctions easily explain why no NIR sources are detected toward the G34.4 MM core. Similarly, the NIR sources seen in the neighborhood of the southern core are probably located at its periphery and not at its center.

4.4. *Circumstellar Material around Members of the NIR Cluster*

As discussed in § 3, Figures 5 and 6 show that about 50% of cluster members with *JHK′* detections have NIR colors clearly offset from those of main-sequence stars, suggesting the presence of circumstellar gas and dust (albeit below our millimeter continuum detection limit). Observational evidence for the presence of disks in clusters of varying ages suggests that

TABLE 3
$H^{13}CO^+$ ($J = 1\text{–}0$) Mass and Column Density Estimates

Source	Peak Position (J2000.0)	$H^{13}CO^+$ Mass ($M_\odot$)	Average $H^{13}CO^+$ Column Density (10^{14} cm^{-2})	Inferred H_2 Mass ($M_\odot$)
G34.4 MM core	18 53 18.00, +01 25 24.9	9.3×10^{-8}	1.7	4×10^3
Southern core	18 53 18.58, +01 24 50.5	1.3×10^{-7}	2.4	5×10^3
Total[a]	...	1.1×10^{-6}	1.3	5×10^4

Note.—Units of right ascension are hours, minutes, and seconds, and units of declination are degrees, arcminutes, and arcseconds.
[a] Total includes core emission and diffuse component.

in low- and intermediate-mass star-forming regions, half of all stars lose their disks within 3 Myr and 90% of stars lose their disks within 5 Myr (e.g., Robberto et al. 1999; Meyer & Beckwith 2000; Haisch, Lada, & Lada 2001). Low-mass dust disks (as low as 0.1 lunar masses) may even persist as long as a billion years (Spangler et al. 2001).

Only 30% of the members of the NIR cluster are detected in all three bands, and half of those appear to have circumstellar material. Using the relation between the percent of sources with NIR excess in a cluster and the age of the cluster (Haisch et al. 2001), our *JHK′* data suggest that the NIR cluster is less than 3 Myr old. This is consistent with the large number of sources seen in Figure 6 that have $(J-K')$ colors well in excess of the 3 Myr pre–main-sequence locus. How does this estimate compare with estimates of disk dispersal times?

The most massive star in the NIR cluster (source 54) has an infrared excess, suggesting that it still has circumstellar material. Assuming that the material resides in a disk, how long would it take for this star to photoevaporate its disk? Using the "weak-wind" model of Hollenbach et al. (1994), the lifetime of a circumstellar disk is given by

$$\tau_{\rm disk} = 7 \times 10^4 \Phi_{49}^{-1/2} M_1^{-1/2} M_d \text{ yr}, \quad (1)$$

where (1) Φ_{49} is the ionizing Lyman continuum flux in units of 10^{49} s^{-1}, (2) M_1 is the mass of the central star in units of 10 $M_\odot$, and (3) M_d is the disk mass in units of $M_\odot$. For source 54 we assume $M_* = 5\ M_\odot$, $\Phi_{49} \sim 8 \times 10^{-7}$ (Thompson 1984), and $M_1 \sim 0.5$. Shu et al. (1990) showed that an accretion disk becomes gravitationally unstable when it reaches a mass of $M_d \sim 0.3 M_*$, where M_* is the mass of the central protostar. During the initial collapse of the cloud core, the disk mass may be maintained close to the value of $0.3 M_*$. When infall ceases and the disk mass falls below the critical value, disk accretion onto the star may rapidly decline, and photoevaporation may be the dominant mechanism that disperses the remaining gas and dust (Hollenbach et al. 1994). Based on this scenario, we assume an initial disk at the edge of stability, that is, $M_d \sim 0.3 M_* = 1.5\ M_\odot$. Errors in the estimate for the photoevaporative timescale would scale directly as M_d. We find that $\tau_{\rm disk} \sim 10^8$ yr. For the less luminous stars in the cluster, the photoevaporative timescale would be significantly longer. Thus, circumstellar disks should persist in the IRAS 18507 star-forming region for at least 10^8 yr.

5. SUMMARY

Two massive molecular cores are detected toward IRAS 18507. The northern molecular core is associated with a newly discovered millimeter continuum peak, G34.4 MM, produced by a mixture of thermal dust emission (56.3 mJy) and ionized gas emission (0.52 mJy). Several hundred solar masses of warm gas and dust surround the central B2 star. The high mass of warm circumstellar material is consistent with the lack of detection at NIR wavelengths and suggests that the source is, perhaps, younger than those near the southern molecular core and may represent the relatively rare case of a massive protostar (e.g., analogous to low-mass Class 0 protostars). If the central protostar is undergoing accretion typical of early B protostars (e.g., $\dot{M}_{\rm acc} \sim 10^{-5}$ to 10^{-3}), then there might be significant dust absorption within the H II region, or the emission might be quenched by high accretion rates; both conditions would tend to underestimate the spectral type of the embedded protostar (e.g., Churchwell 1999 and references therein).

The southern core is associated with an NIR cluster of young stars and a UC H II region, G34.4+0.23, with a central B0.5 star. No millimeter continuum emission is detected toward the peak of the UC H II region, suggesting that the source has had time to disperse a significant fraction of the warm gas and dust that typically enshrouds protostars during their early evolutionary phase. The molecular core has not been destroyed by the forming stars; instead, the stars appear to have formed around the periphery of the core, leaving the core itself intact. Further observations searching for outflowing gas at millimeter wavelengths toward both molecular cores would help constrain the relative age of the sources in IRAS 18507.

Only 30% of stars in the NIR stellar cluster are seen in all NIR bands. Of those, 50% have excess emission, suggesting the presence of at least some circumstellar material (well below our millimeter continuum detection limit). On the basis of the fraction of stars with NIR excess, we estimate that the cluster is less than 3 Myr old.

Research at the Owens Valley Radio Observatory is supported by the National Science Foundation through NSF grant AST 96-13717. Star formation research at Owens Valley is also supported by NASA's Origins of Solar Systems program, grant NAGW-4030, and by the Norris Planetary Origins Project. L. B. acknowledges support by FONDECYT grant 1010431 and by Centro de Astrofísica FONDAP 15010003.

REFERENCES

Blake, G. A., Sutton, E. C., Masson, C. R., & Phillips, T. G 1987, ApJ, 315, 621
Bohlin, R. C., Savage, B. D., & Drake, J. F. 1978, ApJ, 224, 132
Bronfman, L., Nyman, L.-Å., & May, J. 1996, A&AS, 115, 81
Carral, P., & Welch, W. J. 1992, ApJ, 385, 244
Churchwell, E. 1999, in The Origin of Stars and Planetary Systems, ed. C. J. Lada & N. D. Kylafis (Dordrecht: Kluwer), 515
Dickman, R. L. 1978, ApJS, 37, 407
Frerking, M. A., Langer, W. D., & Wilson, R. W. 1982, ApJ, 262, 590
Haisch, K. E., Jr., Lada, E. A., & Lada, C. J. 2001, ApJ, 553, L153
Harju, J., Lehtinen, K., Booth, R. S., & Zinchenko, I. 1998, A&AS, 132, 211
Hildebrand, R. H. 1983, QJRAS, 24, 267
Hogerheijde, M. R., van Dishoeck, E. F., Blake, G. A., & van Langevelde, H. J. 1998, ApJ, 502, 315
Hollenbach, D., Johnstone, D., Lizano, S., & Shu, F. 1994, ApJ, 428, 654
Koornneef, J. 1983, A&A, 128, 84
Kramer, C., Alves, J., Lada, C., Lada, E., Sievers, A., Ungerechts, H., & Walmsley, M. 1998, A&A, 329, L33
Meyer, M. R., & Beckwith, S. V. W. 2000, in *ISO* Survey of a Dusty Universe, ed. D. Lemke, M. Stickel, & K. Wilke (LNP 548; Berlin: Springer), 341
Miralles, M. P., Rodríguez, L. F., & Scalise, E. 1994, ApJS, 92, 173
Molinari, S., Brand, J., Cesaroni, R., & Palla, F. 1996, A&A, 308, 573
Molinari, S., Brand, J., Cesaroni, R., Palla, F., & Palumbo, G. G. C. 1998, A&A, 336, 339
Nürnberger, D. E. A. 2003, A&A, 404, 255
Palla, F., Brand, J., Cesaroni, R., Comoretto, G., & Felli, M. 1991, A&A, 246, 249
Palla, F., & Stahler, S. W. 1993, ApJ, 418, 414
Panagia, N. 1973, AJ, 78, 929
Persson, S. E., Murphy, D. C., Krzeminski, W., Roth, M., & Rieke, M. J. 1998, AJ, 116, 2475
Persson, S. E., West, S. C., Carr, D. M., Sivaramakrishnan, A., & Murphy, D. C. 1992, PASP, 104, 204
Pollack, J. B., Hollenbach, D., Beckwith, S., Simonelli, D. P., Roush, T., & Fong, W. 1994, ApJ, 421, 615
Ramesh, B., Bronfman, L., & Deguchi, S. 1997, PASJ, 49, 307

Richards, P. J., Little, L. T., Toriseva, M., & Heaton, B. D. 1987, MNRAS, 228, 43
Rieke, G. H., & Lebofsky, M. J. 1985, ApJ, 288, 618
Robberto, M., Meyer, M. R., Natta, A., & Beckwith, S. V. W. 1999, in The Universe as Seen by *ISO*, ed. P. Cox & M. F. Kessler (ESA-SP 427; Noordwijk: ESA), 195
Saraceno, P., André, P., Ceccarelli, C., Griffin, M., & Molinari, S. 1996, A&A, 309, 827
Sault, R. J., Teuben, P. J., & Wright, M. C. H. 1995, in ASP Conf. Ser. 77, Astronomical Data Analysis Software and Systems IV, ed. R. A. Shaw, H. E. Payne, & J. J. E. Hayes (San Francisco: ASP), 433
Scalise, E., Jr., Rodríguez, L. F., & Mendoza-Torres, E. 1989, A&A, 221, 105
Schutte, A. J., van der Walt, D. J., Gaylard, M. J., & MacLeod, G. C. 1993, MNRAS, 261, 783
Scoville, N. Z., Carlstrom, J. E., Chandler, C. J., Phillips, J. A., Scott, S. L., Tilanus, R. P. J., & Wang, Z. 1993, PASP, 105, 1482
Shepherd, D. S., & Watson, A. M. 2002, ApJ, 566, 966
Shu, F. H., Tremaine, S., Adams, F. C., & Ruden, S. P. 1990, ApJ, 358, 495
Spangler, C., Sargent, A. I., Silverstone, M. D., Becklin, E. E., & Zuckerman, B. 2001, ApJ, 555, 932
Strom, K. M., Strom, S. E., & Merrill, K. M. 1993, ApJ, 412, 233
Szymczak, M., Hrynek, G., & Kus, A. J. 2000, A&AS, 143, 269
Thompson, R. I. 1984, ApJ, 283, 165
Wilson, T. L., & Rood, R. T. 1994, ARA&A, 32, 191
Wood, D. O. S., & Churchwell, E. 1989, ApJS, 69, 831